HHS Public Access

Author manuscript

Sci Transl Med. Author manuscript; available in PMC 2024 June 07.

Published in final edited form as:

Sci Transl Med. 2023 December 20; 15(727): eadf8366. doi:10.1126/scitranslmed.adf8366.

Inhibition of RIP1 improves immune reconstitution and reduces GVHD mortality while preserving graft-versus-leukemia effects

Mariano Prado-Acosta[1,†], **Seihwan Jeong**[1,†], **Alberto Utrero-Rico**[1], **Tatiana Goncharov**[2], **Joshua D. Webster**[3], **Ernst Holler**[4], **George Morales**[1], **Sergio Dellepiane**[1], **John E. Levine**[1], **Michael E. Rothenberg**[5], **Domagoj Vucic**[2,‡], **James L. M. Ferrara**[1,*,‡]

[1]Tisch Cancer Institute, Icahn School of Medicine at Mount Sinai, New York, NY 10029, USA.

[2]Immunology Discovery, Genentech, South San Francisco, CA 94080, USA.

[3]Department of Pathology, Genentech, South San Francisco, CA 94080, USA.

[4]Department of Hematology and Oncology, University of Regensburg, Regensburg 93042, Germany.

[5]Early Clinical Development, Genentech, South San Francisco, CA 94080, USA.

Abstract

Graft-versus-host disease (GVHD) remains the major cause of morbidity and nonrelapse mortality (NRM) after hematopoietic cell transplantation (HCT). Inflammatory cytokines mediate damage to key GVHD targets such as intestinal stem cells (ISCs) and also activate receptor interacting protein kinase 1 (RIP1; RIPK1), a critical regulator of apoptosis and necroptosis. We therefore investigated the role of RIP1 in acute GVHD using samples from HCT patients, modeling GVHD damage in vitro with both human and mouse gastrointestinal (GI) organoids, and blocking RIP1 activation in vivo using several well-characterized mouse HCT models. Increased phospho-RIP1 expression in GI biopsies from patients with acute GVHD correlated with tissue damage and predicted NRM. Both the genetic inactivation of RIP1 and the RIP1 inhibitor GNE684 prevented GVHD-induced apoptosis of ISCs in vivo and in vitro. Daily administration of GNE684 for 14 days reduced inflammatory infiltrates in three GVHD target organs (intestine, liver, and spleen) in mice. Unexpectedly, GNE684 administration also reversed the marked loss of regulatory

*Corresponding author. james.ferrara@mssm.edu.
†These authors contributed equally to this work.
‡These authors contributed equally to this work.

Author contributions: Conceptualization: J.L.M.F., D.V., S.J., and M.P.-A. Formal analysis: M.P.-A., S.J., and A.U.-R. Methodology: J.L.M.F., D.V., J.D.W., and M.E.R. Investigation: M.P.-A., S.J., A.U.-R., G.M., S.D., and T.G. Visualization: M.P.-A., A.U.-R., J.L.M.F., D.V., and T.G. Funding acquisition: J.L.M.F., D.V., and J.E.L. Project administration: J.L.M.F. and D.V. Supervision: J.L.M.F. and D.V. Writing—original draft: J.L.M.F. and M.P.-A. Writing—review and editing: S.J., A.U.-R., J.D.W., S.D., E.H., J.E.L., M.E.R., and D.V.

Competing interests: J.L.M.F. consultancies: Alexion, Editas, Equillium, Incyte, Medpace, Moderna, Mesoblast, Realta, and Viracor. J.E.L. research support: Equillium, Incyte, MaaT Pharma, and Mesoblast; consultancies: Equillium, Inhibrx, Kamada, Mesoblast, and Sanofi. E.H. consultancies: MaatPharma, Pharmabiome, Medac, and Novartis. T.G., J.D.W., M.E.R., and D.V. own stock shares of Genentech/Roche. All other authors declare that they have no competing interests.

Data and materials availability: All data associated with this study are present in the paper or the Supplementary Materials. GNE684 and Ripk1D138N/D138N mice were provided by Genentech under a material transfer agreement.

T cells in the intestines and liver during GVHD and reduced splenic T cell exhaustion, thus improving immune reconstitution. Pharmacological and genetic inhibition of RIP1 improved long-term survival without compromising the graft-versus-leukemia (GVL) effect in lymphocytic and myeloid leukemia mouse models. Thus, RIP1inhibition may represent a nonimmunosuppressive treatment for GVHD.

Editor's summary

Allogeneic hematopoietic cell transplantation (HCT) is performed for patients with leukemia to induce graft-versus-leukemia (GVL) effects. However, the GVL effect is closely tied to development of graft-versus-host disease (GVHD), and GVHD treatments can limit GVL effects. Here, Prado-Acosta and colleagues studied the role of receptor interacting protein kinase 1 (RIP1) in acute GVHD, finding that increased phospho-RIP1 was associated with worsened intestinal damage and increased nonrelapse mortality in patients undergoing allogeneic HCT. In mice undergoing HCT, genetic knockout or pharmacological inhibition of RIP1 was associated with decreased intestinal damage and improved survival. RIP1 inhibition also improved immune reconstitution in mice undergoing allogeneic HCT and did not inhibit GVL effects in leukemic mice, suggesting that RIP1 inhibition may be a nonimmunosuppressive treatment for GVHD.
—Melissa L. Norton

INTRODUCTION

Receptor interacting protein kinase 1 (RIP1; RIPK1) is a critical regulator of inflammatory cell death and mediator of multiple signaling pathways downstream of tumor necrosis factor receptor 1 (TNFR1) (1, 2). Stimulation with TNFα initially leads to RIP1 engagement in the TNFR1 signaling complex (I) and nuclear factor kappa light chain enhancer of activated B cell (NF-kB) activation (3). However, when RIP1 dissociates from complex I, it subsequently associates with caspase-8 and RIP3 in cytoplasmic complexes (II) to mediate apoptotic and necroptotic cell death (3). Within complex II, RIP1 undergoes autophosphorylation, triggering its activation and downstream cell death signaling (4-6). The kinase activity of RIP1 is an attractive therapeutic target because it is critical to cell death mediated by TNFα and other inflammatory stimuli with no known risk of immunosuppression (7-9). It is also amenable to small-molecule inhibition, and to date, several RIP1 kinase inhibitors have been used in animal models, where they reduced the severity of skin disease, arthritis, kidney damage, and myocardial damage (7, 9, 10). Jointly, these data have defined the role of RIP1 in a number of inflammatory conditions, including ileocolitis, renal disease, and neurodegenerative disorders such as multiple sclerosis (1, 8, 10-12).

TNFα is an important mediator of inflammatory bowel disease, and recent research has focused on the role of RIP1 in damage to gastrointestinal (GI) epithelium (10, 13-15). RIP1 activation is required for death of cells in the intestinal crypts, which can be prevented both by genetic inactivation of the RIP1 kinase domain and by pharmacologic inhibition (14). RIP1 inhibition can prevent damage to the intestinal mucosa when the epithelium is susceptible to inflammatory stimuli, for example, in disorders with genetic mutations in autophagy regulators such as autophagy related 16 like 1 (*ATG16L1*) (15) or in NF-kB

essential modulator (*NEMO*) (10). RIP1 inhibitors that maintain the RIP1 kinase in an inactive conformation are now under clinical investigation for the treatment of several diseases, including psoriasis and inflammatory bowel disease (7, 14-18).

Allogeneic hematopoietic cell transplantation (HCT) relies on the powerful graft-versus-leukemia (GVL) effect to eradicate hematologic malignancies. The GVL effect is tightly linked, however, to graft-versus-host disease (GVHD), the major cause of early nonrelapse mortality (NRM) after HCT. The GI tract is a key target organ of GVHD, and the need for enhanced regeneration of the GI crypt to improve long-term GVHD outcomes is well established (19-22).

We hypothesized that RIP1 is activated during GVHD and that inhibiting RIP1 activation would protect key GVHD target organs such as the intestine and liver without suppressing the immune system. Here, we showed strong RIP1 phosphorylation (pRIP1) during GVHD-induced damage of the intestines using biopsies from HCT patients and correlation of RIP1 phosphorylation with NRM. We also observed RIP1-mediated cell death during GVHD damage in human and mouse intestinal organoid models that could be reversed by treatment with a RIP1 inhibitor. Using in vivo mouse models of GVHD that used genetic and pharmacologic approaches to inactivate/inhibit RIP1 kinase activity, we demonstrated that RIP1 inhibition could modulate GVHD effects while maintaining a GVL benefit. Therefore, inhibition of RIP1 may be a potential treatment for acute GVHD in patients.

RESULTS

RIP1 activation correlates with GVHD damage in human intestinal biopsies and correlates with long-term patient outcomes

To evaluate the relevance of the RIP1 pathway in clinical acute GVHD, we measured RIP1 by quantifying its phosphorylation (pRIP1) in GI biopsy samples from 24 patients who underwent HCT using a previously established four-point scale (Fig. 1A and fig. S1) (10, 23). We found a strong correlation between pRIP1 abundance and histologic damage as measured by the Lerner score (Fig. 1B). In addition, the area under the receiver operator characteristic curve of pRIP1 abundance and NRM within 12 months of biopsy was 0.81 (Fig. 1C). The cumulative incidence of 12-month NRM in patients with moderate or marked pRIP1 levels (two or three of a three-point semiquantitative scale by immunohistochemistry) was fivefold higher than that in patients with rare or no pRIP1 (Fig. 1D). All patients who died, died from GVHD.

Inactivation of RIP1 rescues human and mouse intestinal organoids from apoptosis

We next evaluated the role of the RIP1 pathway in GVHD damage using human intestinal organoid cultures. Sera from seven individual patients with GI GVHD (table S1) contained elevated concentrations of interferon-γ (IFN-γ) and TNFα (Fig. 2A), and the addition of individual serum samples to culture media markedly reduced the viability of third-party human organoids, which could be reversed by the addition of RIP1 inhibitor GNE684 (Fig. 2, B and C, and fig. S2A). The addition of 10 ng/ml of IFN-γ or TNFα alone did not adversely affect organoid growth (fig. S2A), but their combination caused a substantial loss

of organoid viability that was also reversed by GNE684 (Fig. 2, D and E). The addition of the pancaspase inhibitor emricasan (24) improved organoid viability, but the combination of GNE684 and emricasan did not cause further improvement, suggesting that the TNFα and IFN-γ in serum reduced organoid viability primarily by apoptosis. GNE684 also reversed the phosphorylation of RIP1 when the inhibitor of apoptosis antagonist birininapant was added to TNFα in human colon organoids (Fig. 2F).

We next used the well-defined C3H.SW → B6 murine model to evaluate the role of RIP1 in GI damage during GVHD. Similar to observations in human samples, serum obtained from individual mice on day +9 after allogeneic HCT markedly reduced the viability of organoids established from the ilea of naïve B6 mice, and the addition of GNE684 to the culture media significantly ($P < 0.001$) improved organoid viability (Fig. 3A and fig. S2B). As expected, serum from mice with GVHD contained increased concentrations of IFN-γ and TNFα (fig. S3); the addition of both IFN-γ and TNFα reduced organoid viability in a dose-dependent fashion that was also significantly ($P < 0.001$) reversed by GNE684 (Fig. 3B). Emricasan similarly improved organoid viability, but the combination of GNE684 and emricasan did not result in further improvement (Fig. 3, C to F), again suggesting that the loss of organoid viability was due primarily to apoptosis.

Intestinal stem cells (ISCs) are key targets of GVHD (25, 26). To evaluate the effect of RIP1 inhibition on the fate of ISCs, we quantified the effects of IFN-γ and TNFα on $Lgr5^+$ ISCs in organoids derived from Lgr5-eGFP mutant mice, where the number of $Lgr5^+$ ISCs is highly correlated with the organoid viability (fig. S2B). The two inflammatory cytokines in culture media reduced the number of $Lgr5^+$ ISCs by 50%, which was reversed by both GNE684 and emricasan to the same degree (Fig. 3C). Inhibition of RIP1 and caspase inactivation afforded similar protection to sorted single $Lgr5^+$ ISCs cultured as nascent organoids for 72 hours (Fig. 3D). We observed similar beneficial effects of RIP1 and caspase inhibition in parallel analyses of organoids that were treated with GNE684 or that were established from B6 $Ripk1^{D138N/D138N}$ (RIP1 KD) mice in which RIP1 kinase was genetically inactivated (23) (Fig. 3, E and F). Together, these data showed that RIP inhibition rescued ISCs from apoptosis mediated by inflammatory cytokines produced during GVHD.

Genetic inactivation of RIP1 in mice prevents GI GVHD and reduces mortality after HCT

The observations in organoids using serum samples from patients and mice with GVHD led us to evaluate the role of RIP1-mediated cell death in well-characterized mouse models of acute GVHD. We first analyzed the GI tract on days +9 and + 10 after syngeneic (B6 → B6) and allogeneic (C3H.SW → B6) HCT. Western blots of the ileum showed cleavage of caspase 3 in wild-type (WT) recipients of allogeneic HCT but not in RIP1 kinase dead (KD) recipients (Fig. 4, A and B). In RIP1 KD mice, the aspartic acid at position 138 of the kinase has been mutated to an asparagine, preventing its activation (10). There was no evidence of phosphorylated RIP3 or phosphorylated mixed lineage kinase-like (MLKL) in these samples (Fig. 4A), supporting apoptosis rather than necroptosis as the primary form of cell death during GVHD. GVHD in WT recipients caused 10-fold increases in the numbers of both $CD4^+$ and $CD8^+$ lamina propria lymphocytes secreting TNFα, IFN-γ, and IL-17 that returned to baseline syngeneic HCT concentrations in KD recipients (Fig. 4, C and D, and

fig. S4, A and B). Intestinal length improved in KD mice, which resulted in significantly ($P < 0.001$) diminished GVHD mortality (Fig. 4, E and F). We observed a similar reduction in mortality using Balb/c donors to induce GVHD (Fig. 4G).

Pharmacological inhibition of RIP1 by GNE684 prevents GI GVHD and improves survival in mice

We next evaluated the ability of pharmacologic inhibition of RIP1 to control GVHD by daily intraperitoneal administration of GNE684 (75 mg/kg) from the day of HCT in the C3H.SW → B6 model. Phenotypic analysis of lamina propria lymphocytes taken from the small intestine during GVHD showed that GNE684 administration markedly reduced the number of effector $CD4^+$ T cells ($CD4^+IFN\text{-}\gamma^+$ and $CD4^+TNF\alpha^+$), effector $CD8^+$ T cells ($CD8^+IFN\text{-}\gamma^+$ and $CD8^+TNF\alpha^+$), macrophages ($F4/80^+$), natural killer cells ($NK1.1^+$), and neutrophils ($Ly6G^+$) (Fig. 5A and fig. S5). GNE684 administration also markedly increased the number of regulatory T cells [T_{regs}; ($CD4^+Foxp3^+$)] so that the $CD4^+$ T_{reg}/conventional $CD4^+FoxP3^-$ T cell (Tcon) ratio returned to syngeneic HCT ratios (Fig. 5A). GNE684 treatment reversed the loss of $Lgr5^+$ ISCs in the intestinal crypts, which correlated with restored intestinal length (Fig. 5, B and C). Culture of freshly isolated intestinal crypts from mice with GVHD on day +9 after HCT showed that both GNE684 and emricasan added in vitro significantly ($P < 0.001$) improved organoid viability from crypts of mice with GVHD; the addition of both compounds did not cause further improvement, however, providing further evidence that RIP1 inhibition acts to prevent the apoptosis of ISCs (Fig. 5D). Daily intraperitoneal administration of GNE684 for 14 days reduced mortality from GVHD in a dose-dependent fashion in two donor/recipient strain combinations (Fig. 5, E and F). GNE684 administration also reversed acute GVHD mortality when its administration was delayed until day +7 at a time when GVHD was already advanced (Fig. 5G).

RIP1 inhibition improves immune reconstitution during GVHD in mice

To determine whether the reduction in inflammatory cellular infiltrates caused by GNE684 was limited to the GI tract, we performed a similar analysis of cellular infiltrates in a second GVHD target organ, the liver. We again observed reductions in effector $CD4^+$ T cells ($CD4^+IFN\text{-}\gamma^+$ and $CD4^+TNF\alpha^+$), effector $CD8^+$ T cells ($CD8^+IFN\text{-}\gamma^+$ and $CD8^+TNF\alpha^+$), macrophages ($F4/80^+$), natural killer cells ($NK1.1^+$), and neutrophils ($Ly6G^+$) (Fig. 6). We also observed the same marked increase in T_{regs} ($CD4^+FoxP3^+$) and restoration of the $CD4^+$ T_{reg}/Tcon ratio to syngeneic HCT levels.

We next explored different approaches to determine whether RIP1 inhibition generally suppressed overall lymphocyte function. Addition of GNE684 to mixed lymphocyte reactions in vitro resulted in no change in the proliferation or cytokine production of either $CD4^+$ or $CD8^+$ responding T cells (Fig. 7A). Daily administration of GNE684 for 14 days after syngeneic HCT had no effect on thymocyte subset number or distribution at a time when the thymus is rapidly regenerating (Fig. 7B). In addition, both $CD4^+$ and $CD8^+$ splenic lymphocytes responded normally to CD3/CD28 stimulation (Fig. 7C). Thus, RIP1 inhibition had no effect on acute activation of T cells in the absence of GVHD. Analysis of both syngeneic and allogeneic HCT recipient mice showed fewer effector T cells and more T_{regs} in the spleen after GNE684 treatment, similar to results in the intestine and liver (fig. S6).

GNE684 treatment also reduced two markers of T cell exhaustion, programmed cell death protein 1 (PD-1), and T cell immunoglobulin and mucin domain 3 (TIM-3), on both $CD4^+$ and $CD8^+$ T cells, which correlated with improved proliferation and cytokine secretion to third-party (Balb/c) allogeneic dendritic cells (DCs) (Fig. 7D and fig. S7).

Inhibition of RIP1 preserves GVL effect in mice

The clinical benefit of allogeneic HCT derives from the beneficial GVL effect that is closely associated with GVHD (27). We therefore used well-characterized models of lymphoid malignancy (EL4) and myeloid malignancy (C1498) that are syngeneic to B6 recipient mice to determine whether RIP1 inhibition had any impact on GVL effects (28). Tumor cells were injected together with the donor inoculum to mimic residual leukemia burden that persists after HCT conditioning. All syngeneic HCT recipients died of leukemia within 3 weeks of injection (Fig. 8, A to D, left). HCT recipients of allogeneic C3H.SW donor grafts rejected both tumors, demonstrating substantial GVL effects. Most B6 WT recipients, however, died from GVHD, whereas most recipient mice in which RIP1 was inhibited survived, whether the inhibition was through genetic inactivation in B6-RIP1 KD recipients or though pharmacologic inactivation by daily injections of GNE684 (Fig. 8, A to D, right). Thus, inhibition of RIP1 successfully prevented GVHD while preserving beneficial GVL effects in mice.

DISCUSSION

Here, we found that RIP1 inhibition prevented GVHD by rescuing ISCs from apoptosis while preserving GVL effects and improving immune reconstitution. The GI tract is considered the most critical of the three acute GVHD target organs because GVHD is hardest to control in the GI tract and its response to therapy largely determines long-term outcomes such as survival (29-31). Histologic severity of GVHD in the lower GI tract is characterized by apoptotic cells near the crypt base, with crypt loss in severe cases (32-34). Immunologic homeostasis in the GI tract involves complex regulation of both innate and adaptive immune responses that must distinguish between potentially pathogenic species among the trillions of bacteria in the gut lumen and prevent unwanted inflammatory responses to food-borne antigens (27, 35).

Preclinical models of GVHD have confirmed that $Lgr5^+$ ISCs are key targets of acute GVHD (25, 26). ISCs proliferate rapidly during GVHD but are unable to regenerate the epithelial barrier because they rapidly undergo apoptosis (26). Destruction of the crypt by GVHD accelerates the erosion of ISC reserve with the loss of Paneth cells that are critical for regeneration of the mucosal epithelial surface (36-38). The loss of Paneth cells in biopsies correlates with severe GVHD (15, 39, 40), whereas restoration of Paneth cell function attenuates GVHD (34, 38, 41).

GVHD physiology is characterized by the production of inflammatory effector cytokines, particularly IFN-γ and TNFα (27, 35), and we modeled GVHD damage to intestinal crypts in both human and mouse organoids using a combination of these two cytokines. IFN-γ leads to Paneth cell death and causes extrusion from organoids, irreversibly damaging the crypt (42-44). TNFα also prevents regeneration of the intestinal epithelium during GVHD

when ISCs are susceptible to inflammatory injury (29, 44). Our data show that sera from individuals with GVHD cause RIP1-dependent apoptosis in intestinal organoids that is replicated by the combination of IFN-γ and TNFα. Our results largely confirm those of a recent study reporting the rescue of mice from lethal GVHD using a different RIP1 inhibitor (45). The absence of activation of RIP3 and MLKL in our study is consistent with the lack of MLKL-dependent necroptosis observed in that study and with the observation that apoptosis is the histological hallmark of acute GVHD damage (32). Together with the equivalent ability of RIP1 inhibition by GNE684 and caspase inhibition by emricasan to rescue ISCs in vitro, as well as the lack of synergism between these two inhibitors, we conclude that RIP1 inhibition prevents the apoptosis of intestinal targets of GVHD.

Recent GVHD research has come to appreciate the critical importance of repair and regulation of the GI epithelium in this disease process (22). This emphasis on the regulative capacity of the GI tract is consistent with the notion of tissue tolerance or resistance to immunologic attack that has been proposed as a critical contributor to GVHD damage (46). Our data show that pharmacologic inhibition of RIP1 prevents GVHD to the same extent as genetic inactivation of RIP1 in HCT recipients and that both approaches dramatically reduce the infiltration of inflammatory effector cells into intestinal tissues. Unexpectedly, RIP1 kinase inhibition also resulted in marked increases in T_{regs} in GVHD target organs and the restoration of immunologic homeostasis. T cell exhaustion during GVHD has been well described (47, 48), and GNE684 treatment reduced the expression of two T cell exhaustion markers and improved T cell functional responses to third-party alloantigens. We hypothesize that the effect of RIP1 kinase inhibition on T_{regs} is indirect, and it is known that the reversal of dysbiosis can reduce GVHD and induce the expansion of T_{regs} (49, 50). Although the precise mechanism remains to be elucidated, RIP1 inhibition that protected the GI tract from GVHD damage actually improved immune reconstitution, unlike current immunosuppressive treatments such as systemic steroids or calcineurin inhibitors.

RIP1 kinase inhibition of cell death during GVHD, enhancing target organ resistance without suppressing the immune system, is an attractive strategy for two major reasons. First, the therapeutic efficacy of allogeneic HCT relies on the graft-versus-leukemia (GVL) effect to eliminate residual malignancy that was not completely eradicated by the HCT preparative regimen; loss of GVHD may entail loss of GVL effects and increase the risk of relapse. We have shown that a RIP1 inhibitor reduces GVHD while preserving GVL in two different leukemia models, suggesting that this approach will be attractive for patients needing allogeneic HCT. Second, the immune systems of patients with GVHD are usually in the early stages of reconstitution, and GVHD treatment with systemic corticoids substantially increases the risk of serious infections (22).

Our study has several limitations. First, these mouse models use young, healthy mice as HCT recipients, whereas most HCT patients are at least 50 years old and have previously received cytotoxic drugs, which may attenuate the role of apoptosis as the predominant cell death pathway during GVHD. Second, we modeled ISC apoptosis using only two inflammatory cytokines, IFN-γ and TNFα. Other inflammatory cytokines, and other cytolytic pathways such as granzyme/perforin or Fas/Fas ligand, may also attenuate the role of apoptosis in GVHD. Third, although inhibition of RIP1 with GNE684 did not suppress

lymphocyte function either in vitro or in vivo, these experiments were not performed together with other immunosuppressive medications such as calcineurin inhibitors or corticosteroids. Patients with GVHD commonly receive such medications and may be more immunosuppressed than these mouse models suggest. Therefore, these findings should be extrapolated to clinical HCT scenarios with caution.

The importance of RIP1 kinase activity has been demonstrated in a number of animal disease models by using RIP1 KD mice or various RIP1 kinase inhibitors (1, 8, 10, 14, 15, 51-54). These preclinical data positioned RIP1 inhibitors as attractive reagents to test in clinical settings (1, 7, 55). Several clinical trials with RIP1 inhibitors have recently completed in inflammatory diseases, and a few are still ongoing in neurodegenerative and inflammatory indications (56). According to reports from these trials, the RIP1 inhibitor GSK2982772 did not affect disease outcome in patients with arthritis, ulcerative colitis, or psoriasis (57-59), whereas the studies in patients with ALS have not reported any efficacy results yet (60). Thus, the choice of the right disease in which to test RIP1 inhibitors is of critical importance.

Here, we modeled GVHD damage to human GI crypts and used clinically relevant and translatable animal models of acute GVHD to show the benefit of RIP1 inhibition to ameliorate disease. RIP1 genetic inactivation or chemical inhibition did not affect beneficial GVL effects, in agreement with previous studies where RIP1 inhibition did not affect primary tumor growth or metastases (10). Together, these data point to acute GVHD as an important and relevant disease for clinical testing of RIP1 inhibitors. An ongoing clinical study for the treatment of severe GVHD with a RIP1 inhibitor with equivalent potency characteristics of GNE684 is currently accruing patients (https://clinicaltrials.gov/ct2/show/NCT05673876).

MATERIALS AND METHODS

Study design

The objective of this study was to investigate the role of RIP1 in the damage sustained by ISCs in GVHD both in vivo and in three-dimensional organoid cultures. The number of biological replicates, type of statistical methods used, and *P* values are reported in the figure legends. All human patients provided informed consent for the collection of clinical data and biopsy material in accordance with the Declaration of Helsinki, and studies were conducted under Institutional Review Board/Ethics Committee of University Hospital Regensburg and Mount Sinai Hospital, New York City approval. For animal experiments, HCT was performed in both male and female mice under the Institutional Animal Care and Use Committee (IACUC) protocol (Molecular and Cellular Mechanism of GVHD and GVL-IACUC-2014-0202). Cages of mice were randomly assigned to treatment groups. All in vitro experiments in the main text were carried out at least two times, and no outliers or other data points were excluded from our analyses.

Mice

C57/BL6 (B6; H-2b), Balb/c (H-2d), C3H.SW (H-2b), and B6.Lgr5-eGFP-CreERT2 (Lgr5-eGFP; H-2b) were purchased from the Jackson Laboratory. C57/BL6/Ripk1D138N/D138N were previously described (10, 23). All animal experiments were approved by the Institutional Animal Care Use Committees at Icahn School of Medicine at Mount Sinai.

Organoid establishment and passage

Mice were euthanized, and 20 cm of duodenal intestine and 7 cm of colon were separated from surrounding blood vessels and fat, gently flushed with cold phosphate-buffered saline (PBS), cut longitudinally, and extensively washed with PBS to remove any remaining fecal material. Connective tissue and contaminants were removed from 5-mm intestinal pieces by vigorous repeated pipetting in cold PBS until the supernatant became clear and free of floating debris. Tissue was then incubated in Gentle Dissociation Reagent (STEMCELL Technologies, 07174) at room temperature for 20 min on a rocking platform and allowed to settle by gravity. Supernatant was aspirated and intestinal tissue was resuspended in cold PBS with 0.1% bovine serum albumin (Thermo Fisher Scientific, BP671-1). After 30 s of vigorous pipetting, the supernatant was passed through a 70-μm cell strainer three times. The third fraction was enriched in crypts and centrifuged (300 rpm for 5 min at 4°C), washed with Dulbecco's modified Eagle's medium Nutrient Mixture F-12 (DMEM/F-12) with 15 mM Hepes (STEMCELL Technologies, 36254), and centrifuged again.

To establish organoids, crypts were resuspended in Mouse Intesticul Organoid Growth Medium (STEMCELL Technologies, 6005) to an approximate concentration of 2000 crypts/ml. The mixture (50 μl) was added to Growth Factor Reduced Matrigel (Corning, 356231) at a 1:1 v/v ratio and slowly pipetted into the center of a prewarmed 24-well tissue culture plate (Corning, 3526) to form a dome and then was incubated at 37°C for 1 hour to allow Matrigel polymerization; 500 μl of Intesticult Organoid Growth Medium was then added to cover the dome without disturbing it. Media were changed every 2 to 3 days and organoids were passaged every 7 to 10 days. In some experiments, sorted $Lgr5^+$ ISCs were placed on a thin layer of Matrigel and cultured as previously described (61). Viability was measured after 72 hours.

To passage organoids, media were aspirated and subjected to vigorous pipetting for 30 s with cold PBS disrupted domes. Organoids were washed to remove residual Matrigel and incubated with Gentle Dissociation Reagent (STEMCELL Technologies, 07174) for 20 min at room temperature on a rocking platform. Dissociated organoids were washed in DMEM/F-12 with 15 mM Hepes, resuspended to 2000 crypts/ml, mixed in a ratio 1:1 with Matrigel, and plated as described above. Human 3dGRO Ileum Intestinal Organoids were purchased (Sigma-Aldrich SCC368), and colonic organoids (62) were taken from healthy individuals and cultured in IntestinCult Human Organoid Growth media (STEMCELL Technologies, 0190) as described above and passaged every 7 days.

Quantification of organoid growth

Three days after intestinal organoid passage, recombinant IFN-γ (10 ng/ml; Peprotech, L 2117), mouse recombinant TNFα (10 ng/ml; Peprotech, 315-01A), RIP1 inhibitor GNE684

(10) 20 μM (10 ng/μl), and/or Emricasan 10 nM (Medichem Express, HY-10396) were added to media. In some cultures, Birinapant (100 nM) was added 1 hour before the addition of TNFα. After 72 hours of culture, organoid viability was measured by adding CellTiter-Glo assay reagent (Promega, G7573) to each well of a 96-well plate and incubated for 10 min; 150 μl of the resulting solution was transferred to 96-well white opaque plates (Corning Inc. 3917). Serum from human and murine HCT recipients was added to some cultures in a 1:1 v/v ratio.

Lgr5^{+} ISC isolation

Intestinal crypts from 6- to 8-week-old B6 Lgr5-eGFP mice were harvested as above. Intestines were cut and placed on ice in 10 mM EDTA buffer (Invitrogen, AM9260G) for 30 min with a change of buffer every 10 min. Isolated crypts were filtered through a 70-μm cell strainer and further disaggregated into single cells after a 5-min incubation in TrypLE Express (Gibco, 25200-056) supplemented with 10 μM ROCK inhibitor Y-27632 dihydrochloride (Tocris, 12-541-0) at 37°C. Lgr5^{+} stem cells were sorted in BD FACSAria II Cell Sorter (BD Biosciences).

Hematopoietic cell transplantation

Splenocytes and bone marrow (BM) cells collected from the femurs and tibias of euthanized donor mice were suspended in ammonium-chloride-potassium (ACK) lysis buffer (Gibco, A1049201) for 5 min at room temperature to lyse red blood cells. Recipient mice that were at least 12 weeks old and weighing more than 20 g were given 1100 cGy total body irradiation (day −1). On day 0, irradiated mice were injected with 5×10^6 BM cells and 5×10^6 splenocytes from Balb/c donors or 5×10^6 BM and 50×10^6 splenocytes from C3H. SW donors. In all experiments, BM and splenocytes from syngeneic donors were used to create control groups without GVHD or GVL effects. Mortality of mice after HCT was monitored daily.

GVL assessment

C57BL/6-derived myeloid leukemia cell line C1498 (H-2^{b}) and EL4 (H-2^{b}) mouse lymphoma cell lines were obtained from the American Type Culture Collection (ATCC). All cells were propagated in complete RPMI 1640 GlutaMAX medium (Gibco, 72400146) until exponential growth was achieved. Residual host leukemia was modeled by adding 5×10^5 C1498 or 1×10^6 EL4 cells to the BM and splenocytes inoculum at day 0 of the HCT. Survival was monitored daily.

Isolation of cellular infiltrates

Mice were euthanized, and 10 ml of PBS was slowly perfused via intracardiac injection to cleanse GVHD target organs of peripheral blood as previously described (63). Livers were mechanically disrupted and incubated with collagenase D (Roche, 11088882001) and DNase I (Roche, 10104159001) for 1 hour at 37°C. Samples were filtered with a 70-μm strainer (Corning, 352350) and centrifuged in Percoll (Sigma Aldrich, GE17-0891-01) at 1700 rpm for 30 min at room temperature. Cells were incubated with ACK Lysing buffer (Gibco, A10492-01) for 5 min at room temperature and filtered through a 70-μm

strainer, centrifuged at 1300 rpm for 5 min at 4°C, and resuspended in PBS. Lamina propria lymphocytes from small intestines were isolated as previously described (26).

Flow cytometry

Intestinal organoids generated from Lgr5-eGFP mice were collected and washed with cold PBS to remove Matrigel, followed by dissociation and single-cell suspension. Single-cell suspensions were stained with Live Dead Violet for 10 min (Thermo Fisher Scientific, 62248) and anti-mouse EpCAM (CD326) for 30 min. $Lgr5^+$ ISCs were quantified using a previously described gating strategy (26).

Single-cell suspensions were processed as above and stained with Live/Dead for 10 min at room temperature, washed, and stained with surface target antibodies for 30 min at room temperature. Samples were fixed and permeabilized using Foxp3/Transcription Factor Staining Buffer Set (eBioscience, 00-5523-00) and stained with antibodies for 30 min at room temperature. Samples were analyzed using AURORA Cytek and quantified using FlowJo V10 (Tree Star). Intracellular cytokines were detected by incubating cell suspensions for 4 hours with Cell Stimulation Cocktail (eBioscience, 00-4970-93) and Protein Transport Inhibitor Cocktail (eBioscience, 00-4980-03). All flow cytometry reagents are listed in table S2.

T cell proliferation

Spleens collected from mice were mechanically disrupted, lysed using ACK Lysing buffer (Gibco, A10492-01), and filtered by 70-μm strainers, and T cells were isolated from total splenocytes using the Pan T cell Isolation Kit (Miltenyi Biotec, ref. 130-095-130) as indicated by the manufacturer. T cells were counted and stained with carboxyfluorescein diacetate succinimidyl ester (CFSE; Thermo Fisher Scientific, C34554). CFSE-labeled T cells were plated with either Dynabeads Mouse T-Activator CD3/CD28 (Thermo Fisher Scientific, 11456D) or third-party DCs at a 1:2 ratio for 5 days. DCs were generated from Balb/c bone marrows as previously described (64). At least 85% of DCs were $CD11b^+CD11c^+Ly6C^-Ly6G^-MHCII^{high}CD80^{high}$ by flow cytometry. After 5 days, cells were harvested, stained, and analyzed using LSR Fortessa (BD Biosciences).

Enzyme-linked immunosorbent assay

Enzyme-linked immunosorbent assays (ELISAs) were performed according to the manufacturer's instructions for mouse serum (R&D Systems IFN-γ Quantikine ELISA, MIF00; R&D Systems TNFα Quantikine ELISA kit, MTA00B) and human serum (R&D Systems IFN-γ Quantikine ELISA kit, DIF50C; R&D Systems TNFα Quantikine ELISA kit, DTA00D).

Western blot analysis

Snap-frozen ileal sections were lysed in Triton buffer: 20 mM tris-HCl (pH 7.5), 135 mM NaCl, 1.5 mM $MgCl_2$, 1 mM EGTA, 1% Triton X-100, and Halt Protease and Phosphatase Inhibitor Cocktail (ThermoFisher Scientific) for 30 min on ice and centrifuged at 14,000 rpm for 10 min at 4°C; total protein was resolved on SDS-PAGE and immunoblotted with the indicated antibodies (table S3). Levels of both full-length and processed caspase-3 were

quantified using ImageJ software and normalized to actin for each lane. All antibodies used are listed in table S3.

Immunohistochemistry

Intestinal biopsies were fixed in formalin and embedded in paraffin. pRIP1 immunohistochemistry was performed with the Cell Signaling rabbit monoclonal antibody D1L3S at 0.5 μg/ml on the Benchmark platform (Roche) with CC1 standard retrieval (Roche), Ventana Discovery goat Ig Block, and Optiview Amplification (Roche) with diaminobenzidine chromogen for detection and hematoxylin counterstain. Formalin-fixed, paraffin-embedded HT29 cells and HT29 cells treated with TNF/BV6/zVAD served as a positive control. Replacement of D1L3S antibody with a naïve rabbit antibody (DA1E, Cell Signaling Technology) served as a negative control. Immunohistochemistry was performed on the Discovery XT (Roche) platform with CC1 standard antigen retrieval and OmniMap detection with diaminobenzidine as the chromogen and hematoxylin as the counterstain. A tumor xenograft served as a positive control and primary antibody replacement with a naïve rabbit immunoglobulin G (IgG) antibody (Cell Signaling Technology) served as a negative control.

pRIP1 labeling in human intestinal biopsies was scored according to the following metrics: 0, rare to no labeling; 1, mild perinuclear labeling in lamina propria cells and/or rare crypt cell labeling; 2, moderate perinuclear labeling in lamina propria cells and scattered crypt cell labeling; 3, marked perinuclear labeling in lamina propria cells and multifocal crypt cell labeling.

Statistical analysis

Statistical analysis and graphs were performed and generated using Prism (GraphPad) and R statistical package version 4.0.3 (R Core Team 2020) software. Cumulative incidences of NRM and relapse were calculated using Fine and Gray's method. Differences in cumulative incidences were compared using Gray's test and differences in proportions by χ^2 tests. Survival curves were plotted using Kaplan-Meier estimates and compared using the log-rank test. Unpaired two-tailed *t* test was used for parametric data. All data were tested for normality through application of the *F* test with Prism software, and all tests were two sided. Differences were considered significant when the *P* value was less than 0.05. All studies for which data are presented are representative of at least two independent experiments.

Supplementary Material

Refer to Web version on PubMed Central for supplementary material.

Acknowledgments

We thank colleagues at Mt. Sinai and Genentech for helpful comments and discussions.

Funding:

This work was supported by the National Institutes of Health grants P01 CA 039452 (J.L.M.F. and J.E.L.) and P30 CA196521 (J.L.M.F. and J.E.L.) and the Jose Carreras Foundation (E.H.). A.U.-R. holds a Martin Escudero research grant.

REFERENCES AND NOTES

1. Degterev A, Ofengeim D, Yuan J, Targeting RIPK1 for the treatment of human diseases. Proc. Natl. Acad. Sci. U.S.A 116, 9714–9722 (2019). [PubMed: 31048504]
2. Webster JD, Vucic D, The balance of TNF mediated pathways regulates inflammatory cell death signaling in healthy and diseased tissues. Front. Cell Dev. Biol 8, 365 (2020). [PubMed: 32671059]
3. Kist M, Vucic D, Cell death pathways: Intricate connections and disease implications. EMBO J. 40, e106700 (2021). [PubMed: 33439509]
4. Dannappel M, Vlantis K, Kumari S, Polykratis A, Kim C, Wachsmuth L, Eftychi C, Lin J, Corona T, Hermance N, Zelic M, Kirsch P, Basic M, Bleich A, Kelliher M, Pasparakis M, RIPK1 maintains epithelial homeostasis by inhibiting apoptosis and necroptosis. Nature 513, 90–94 (2014). [PubMed: 25132550]
5. Ting AT, Bertrand MJM, More to life than NF-κB in TNFR1 signaling. Trends Immunol. 37, 535–545 (2016). [PubMed: 27424290]
6. Varfolomeev E, Vucic D, RIP1 post-translational modifications. Biochem. J 479, 929–951 (2022). [PubMed: 35522161]
7. Zarrin AA, Bao K, Lupardus P, Vucic D, Kinase inhibition in autoimmunity and inflammation. Nat. Rev. Drug Discov 20, 39–63 (2021). [PubMed: 33077936]
8. Webster JD, Kwon YC, Park S, Zhang H, Corr N, Ljumanovic N, Adedeji AO, Varfolomeev E, Goncharov T, Preston J, Santagostino SF, Patel S, Xu M, Maher J, McKenzie BS, Vucic D, RIP1 kinase activity is critical for skin inflammation but not for viral propagation. J. Leukoc. Biol 107, 941–952 (2020). [PubMed: 31985117]
9. Mifflin L, Ofengeim D, Yuan J, Receptor-interacting protein kinase 1 (RIPK1) as a therapeutic target. Nat. Rev. Drug Discov 19, 553–571 (2020). [PubMed: 32669658]
10. Patel S, Webster JD, Varfolomeev E, Kwon YC, Cheng JH, Zhang J, Dugger DL, Wickliffe KE, Maltzman A, Sujatha-Bhaskar S, Bir Kohli P, Ramaswamy S, Deshmukh G, Liederer BM, Fong R, Hamilton G, Lupardus P, Caplazi P, Lee WP, van Lookeren Campagne M, Johnson A, McKenzie BS, Junttila MR, Newton K, Vucic D, RIP1 inhibition blocks inflammatory diseases but not tumor growth or metastases. Cell Death Differ. 27, 161–175 (2020). [PubMed: 31101885]
11. Stark K, Goncharov T, Varfolomeev E, Xie L, Ngu H, Peng I, Anderson KR, Verschueren E, Choi M, Kirkpatrick DS, Easton A, Webster JD, McKenzie BS, Vucic D, Bingol B, Genetic inactivation of RIP1 kinase activity in rats protects against ischemic brain injury. Cell Death Dis. 12, 379 (2021). [PubMed: 33828080]
12. Linkermann A, Hackl MJ, Kunzendorf U, Walczak H, Krautwald S, Jevnikar AM, Necroptosis in immunity and ischemia-reperfusion injury. Am. J. Transplant 13, 2797–2804 (2013). [PubMed: 24103029]
13. Liu ZY, Wu B, Guo YS, Zhou YH, Fu ZG, Xu BQ, Li JH, Jing L, Jiang JL, Tang J, Chen ZN, Necrostatin-1 reduces intestinal inflammation and colitis-associated tumorigenesis in mice. Am. J. Cancer Res 5, 3174–3185 (2015). [PubMed: 26693068]
14. Wong J, Garcia-Carbonell R, Zelic M, Ho SB, Boland BS, Yao SJ, Desai SA, Das S, Planell N, Harris PA, Font-Burgada J, Taniguchi K, Bertin J, Salas A, Pasparakis M, Gough PJ, Kelliher M, Karin M, Guma M, RIPK1 mediates TNF-induced intestinal crypt apoptosis during chronic NF-κB activation. Cell. Mol. Gastroenterol. Hepatol 9, 295–312 (2020). [PubMed: 31606566]
15. Matsuzawa-Ishimoto Y, Hine A, Shono Y, Rudensky E, Lazrak A, Yeung F, Neil JA, Yao X, Chen YH, Heaney T, Schuster SL, Zwack EE, Axelrad JE, Hudesman D, Tsai JJ, Nichols K, Dewan MZ, Cammer M, Beal A, Hoffman S, Geddes B, Bertin J, Liu C, Torres VJ, Loke P, van den Brink MRM, Cadwell K, An intestinal organoid-based platform that recreates susceptibility to T-cell-mediated tissue injury. Blood 135, 2388–2401 (2020). [PubMed: 32232483]
16. Garcia-Carbonell R, Yao SJ, Das S, Guma M, Dysregulation of intestinal epithelial cell RIPK pathways promotes chronic inflammation in the IBD gut. Front. Immunol 10, 1094 (2019). [PubMed: 31164887]
17. Duan X, Liu X, Liu N, Huang Y, Jin Z, Zhang S, Ming Z, Chen H, Inhibition of keratinocyte necroptosis mediated by RIPK1/RIPK3/MLKL provides a protective effect against psoriatic inflammation. Cell Death Dis. 11, 134 (2020). [PubMed: 32075957]

18. Gobbetti T, Berger SB, Fountain K, Slocombe T, Rowles A, Pearse G, Harada I, Bertin J, Haynes AC, Beal AM, Receptor-interacting protein 1 kinase inhibition therapeutically ameliorates experimental T cell-dependent colitis in mice. Cell Death Dis. 11, 220 (2020). [PubMed: 32249785]
19. Hayase E, Teshima T, Disruption of gut immune system caused by damage of intestinal stem cells and their niche in graft-versus-host disease after allogeneic hematopoietic stem cell transplantation. Clin. Calcium 27, 829–833 (2017). [PubMed: 28536321]
20. Tsai JJ, Velardi E, Shono Y, Argyropoulos KV, Holland AM, Smith OM, Yim NL, Rao UK, Kreines FM, Lieberman SR, Young LF, Lazrak A, Youssef S, Fu YY, Liu C, Lezcano C, Murphy GF, Na IK, Jenq RR, Hanash AM, Dudakov JA, van den Brink MRM, Nrf2 regulates CD4(+) T cell-induced acute graft-versus-host disease in mice. Blood 132, 2763–2774 (2018). [PubMed: 30381375]
21. Koyama M, Hill GR, The primacy of gastrointestinal tract antigen-presenting cells in lethal graft-versus-host disease. Blood 134, 2139–2148 (2019). [PubMed: 31697827]
22. Chakraverty R, Teshima T, Graft-versus-host disease: A disorder of tissue regeneration and repair. Blood 138, 1657–1665 (2021). [PubMed: 34370823]
23. Dominguez S, Varfolomeev E, Brendza R, Stark K, Tea J, Imperio J, Ngu H, Earr T, Foreman O, Webster JD, Easton A, Vucic D, Bingol B, Genetic inactivation of RIP1 kinase does not ameliorate disease in a mouse model of ALS. Cell Death Differ. 28, 915–931 (2021). [PubMed: 32994544]
24. Lekakis V, Cholongitas E, The impact of emricasan on chronic liver diseases: Current data. Clin. J. Gastroenterol 15, 271–285 (2022). [PubMed: 35000120]
25. Hanash AM, Dudakov JA, Hua G, O'Connor MH, Young LF, Singer NV, West ML, Jenq RR, Holland AM, Kappel LW, Ghosh A, Tsai JJ, Rao UK, Yim NL, Smith OM, Velardi E, Hawryluk EB, Murphy GF, Liu C, Fouser LA, Kolesnick R, Blazar BR, van den Brink MR, Interleukin-22 protects intestinal stem cells from immune-mediated tissue damage and regulates sensitivity to graft versus host disease. Immunity 37, 339–350 (2012). [PubMed: 22921121]
26. Zhao D, Kim YH, Jeong S, Greenson JK, Chaudhry MS, Hoepting M, Anderson ER, van den Brink MR, Peled JU, Gomes AL, Slingerland AE, Donovan MJ, Harris AC, Levine JE, Ozbek U, Hooper LV, Stappenbeck TS, Ver Heul A, Liu T-C, Reddy P, Ferrara JL, Survival signal REG3α prevents crypt apoptosis to control acute gastrointestinal graft-versus-host disease. J. Clin. Invest 128, 4970–4979 (2018). [PubMed: 30106382]
27. Zeiser R, Blazar BR, Acute graft-versus-host disease—Biologic process, prevention, and therapy. N. Engl. J. Med 377, 2167–2179 (2017). [PubMed: 29171820]
28. Lu Y, Meng R, Wang X, Xu Y, Tang Y, Wu J, Xue Q, Yu S, Duan M, Shan D, Wang Q, Wang H, Billiar TR, Xiao X, Chen F, Lu B, Caspase-11 signaling enhances graft-versus-host disease. Nat. Commun 10, 4044 (2019). [PubMed: 31492850]
29. Hill GR, Crawford JM, Cooke KR, Brinson YS, Pan L, Ferrara JL, Total body irradiation and acute graft-versus-host disease: The role of gastrointestinal damage and inflammatory cytokines. Blood 90, 3204–3213 (1997). [PubMed: 9376604]
30. MacMillan ML, Robin M, Harris AC, DeFor TE, Martin PJ, Alousi A, Ho VT, Bolaños-Meade J, Ferrara JL, Jones R, Arora M, Blazar BR, Holtan SG, Jacobsohn D, Pasquini M, Socie G, Antin JH, Levine JE, Weisdorf DJ, A refined risk score for acute graft-versus-host disease that predicts response to initial therapy, survival, and transplant-related mortality. Biol. Blood Marrow Transplant 21, 761–767 (2015). [PubMed: 25585275]
31. Etra A, Gergoudis S, Morales G, Spyrou N, Shah J, Kowalyk S, Ayuk F, Baez J, Chanswangphuwana C, Chen YB, Choe H, DeFilipp Z, Gandhi I, Hexner E, Hogan WJ, Holler E, Kapoor U, Kitko CL, Kraus S, Lin JY, Al Malki M, Merli P, Pawarode A, Pulsipher MA, Qayed M, Reshef R, Rösler W, Schechter T, Van Hyfte G, Weber D, Wölfl M, Young R, Özbek U, Ferrara JLM, Levine JE, Assessment of systemic and gastrointestinal tissue damage biomarkers for GVHD risk stratification. Blood Adv. 6, 3707–3715 (2022). [PubMed: 35443021]
32. Lerner KG, Kao GF, Storb R, Buckner CD, Clift RA, Thomas ED, Histopathology of graft-vs.-host reaction (GvHR) in human recipients of marrow from HL-A-matched sibling donors. Transplant. Proc 6, 367–371 (1974). [PubMed: 4155153]

33. Piguet PF, Grau GE, Allet B, Vassalli P, Tumor necrosis factor/cachectin is an effector of skin and gut lesions of the acute phase of graft-vs.-host disease. J. Exp. Med 166, 1280–1289 (1987). [PubMed: 3316469]
34. Stüber E, Von Freier A, Marinescu D, Fölsch UR, Involvement of OX40-OX40L interactions in the intestinal manifestations of the murine acute graft-versus-host disease. Gastroenterology 115, 1205–1215 (1998). [PubMed: 9797376]
35. Ferrara JL, Smith CM, Sheets J, Reddy P, Serody JS, Altered homeostatic regulation of innate and adaptive immunity in lower gastrointestinal tract GVHD pathogenesis. J. Clin. Invest 127, 2441–2451 (2017). [PubMed: 28581444]
36. Ganz T, Paneth cells—Guardians of the gut cell hatchery. Nat. Immunol 1, 99–100 (2000). [PubMed: 11248797]
37. Sato T, van Es JH, Snippert HJ, Stange DE, Vries RG, van den Born M, Barker N, Shroyer NF, van de Wetering M, Clevers H, Paneth cells constitute the niche for Lgr5 stem cells in intestinal crypts. Nature 469, 415–418 (2011). [PubMed: 21113151]
38. Clevers HC, Bevins CL, Paneth cells: Maestros of the small intestinal crypts. Annu. Rev. Physiol 75, 289–311 (2013). [PubMed: 23398152]
39. Cadwell K, Liu JY, Brown SL, Miyoshi H, Loh J, Lennerz JK, Kishi C, Kc W, Carrero JA, Hunt S, Stone CD, Brunt EM, Xavier RJ, Sleckman BP, Li E, Mizushima N, Stappenbeck TS, Virgin IV HW, A key role for autophagy and the autophagy gene Atg16l1 in mouse and human intestinal Paneth cells. Nature 456, 259–263 (2008). [PubMed: 18849966]
40. Hubbard-Lucey VM, Shono Y, Maurer K, West ML, Singer NV, Ziegler CG, Lezcano C, Motta AC, Schmid K, Levi SM, Murphy GF, Liu C, Winkler JD, Amaravadi RK, Rogler G, Dickinson AM, Holler E, van den Brink MR, Cadwell K, Autophagy gene Atg16L1 prevents lethal T cell alloreactivity mediated by dendritic cells. Immunity 41, 579–591 (2014). [PubMed: 25308334]
41. Hayase E, Hashimoto D, Nakamura K, Noizat C, Ogasawara R, Takahashi S, Ohigashi H, Yokoi Y, Sugimoto R, Matsuoka S, Ara T, Yokoyama E, Yamakawa T, Ebata K, Kondo T, Hiramine R, Aizawa T, Ogura Y, Hayashi T, Mori H, Kurokawa K, Tomizuka K, Ayabe T, Teshima T, R-Spondin1 expands Paneth cells and prevents dysbiosis induced by graft-versus-host disease. J. Exp. Med 214, 3507–3518 (2017). [PubMed: 29066578]
42. Farin HF, Karthaus WR, Kujala P, Rakhshandehroo M, Schwank G, Vries RG, Kalkhoven E, Nieuwenhuis EE, Clevers H, Paneth cell extrusion and release of antimicrobial products is directly controlled by immune cell-derived IFN-γ. J. Exp. Med 211, 1393–1405 (2014). [PubMed: 24980747]
43. Eriguchi Y, Nakamura K, Yokoi Y, Sugimoto R, Takahashi S, Hashimoto D, Teshima T, Ayabe T, Selsted ME, Ouellette AJ, Essential role of IFN-γ in T cell-associated intestinal inflammation. JCI Insight 3, e121886 (2018). [PubMed: 30232288]
44. Takashima S, Martin ML, Jansen SA, Fu Y, Bos J, Chandra D, O'Connor MH, Mertelsmann AM, Vinci P, Kuttiyara J, Devlin SM, Middendorp S, Calafiore M, Egorova A, Kleppe M, Lo Y, Shroyer NF, Cheng EH, Levine RL, Liu C, Kolesnick R, Lindemans CA, Hanash AM, T cell-derived interferon-γ programs stem cell death in immune-mediated intestinal damage. Sci. Immunol 4, eaay8556 (2019). [PubMed: 31811055]
45. Yu X, Ma H, Li B, Ji Y, Du Y, Liu S, Li Z, Hao Y, Tian S, Zhao C, Du Q, Jin Z, Zhu X, Tian Y, Chen X, Sun X, Yang C, Zhu F, Ju J, Zheng Y, Zhang W, Wang J, Yang T, Wang X, Li J, Xu X, Du S, Lu H, Ma F, Zhang H, Zhang Y, Zhang X, Hu S, He S, A novel RIPK1 inhibitor reduces GVHD in mice via a nonimmunosuppressive mechanism that restores intestinal homeostasis. Blood 141, 1070–1086 (2023). [PubMed: 36356302]
46. Wu SR, Reddy P, Tissue tolerance: A distinct concept to control acute GVHD severity. Blood 129, 1747–1752 (2017). [PubMed: 28153825]
47. Senjo H, Harada S, Kubota SI, Tanaka Y, Tateno T, Zhang Z, Okada S, Chen X, Kikuchi R, Miyashita N, Onozawa M, Goto H, Endo T, Hasegawa Y, Ohigashi H, Ara T, Hasegawa Y, Murakami M, Teshima T, Hashimoto D, Calcineurin inhibitor inhibits tolerance induction by suppressing terminal exhaustion of donor T cells after allo-HCT. Blood 142, 477–492 (2023). [PubMed: 37216687]
48. Minnie SA, Waltner OG, Ensbey KS, Nemychenkov NS, Schmidt CR, Bhise SS, Legg SRW, Campoy G, Samson LD, Kuns RD, Zhou T, Huck JD, Vuckovic S, Zamora D, Yeh A, Spencer

A, Koyama M, Markey KA, Lane SW, Boeckh M, Ring AM, Furlan SN, Hill GR, Depletion of exhausted alloreactive T cells enables targeting of stem-like memory T cells to generate tumor-specific immunity. Sci. Immunol 7, eabo3420 (2022). [PubMed: 36240285]

49. Rafei H, Jenq RR, Microbiome-intestine cross talk during acute graft-versus-host disease. Blood 136, 401–409 (2020). [PubMed: 32526029]
50. Atarashi K, Tanoue T, Oshima K, Suda W, Nagano Y, Nishikawa H, Fukuda S, Saito T, Narushima S, Hase K, Kim S, Fritz JV, Wilmes P, Ueha S, Matsushima K, Ohno H, Olle B, Sakaguchi S, Taniguchi T, Morita H, Hattori M, Honda K, Treg induction by a rationally selected mixture of Clostridia strains from the human microbiota. Nature 500, 232–236 (2013). [PubMed: 23842501]
51. Newton K, Dugger DL, Maltzman A, Greve JM, Hedehus M, Martin-McNulty B, Carano RA, Cao TC, van Bruggen N, Bernstein L, Lee WP, Wu X, DeVoss J, Zhang J, Jeet S, Peng I, McKenzie BS, Roose-Girma M, Caplazi P, Diehl L, Webster JD, Vucic D, RIPK3 deficiency or catalytically inactive RIPK1 provides greater benefit than MLKL deficiency in mouse models of inflammation and tissue injury. Cell Death Differ. 23, 1565–1576 (2016). [PubMed: 27177019]
52. Linkermann A, Brasen JH, Himmerkus N, Liu S, Huber TB, Kunzendorf U, Krautwald S, Rip1 (receptor-interacting protein kinase 1) mediates necroptosis and contributes to renal ischemia/reperfusion injury. Kidney Int. 81, 751–761 (2012). [PubMed: 22237751]
53. Saleh D, Najjar M, Zelic M, Shah S, Nogusa S, Polykratis A, Paczosa MK, Gough PJ, Bertin J, Whalen M, Fitzgerald KA, Slavov N, Pasparakis M, Balachandran S, Kelliher M, Mecsas J, Degterev A, Kinase activities of RIPK1 and RIPK3 can direct IFN-β synthesis induced by lipopolysaccharide. J. Immunol 198, 4435–4447 (2017). [PubMed: 28461567]
54. Taraborrelli L, Peltzer N, Montinaro A, Kupka S, Rieser E, Hartwig T, Sarr A, Darding M, Draber P, Haas TL, Akarca A, Marafioti T, Pasparakis M, Bertin J, Gough PJ, Bouillet P, Strasser A, Leverkus M, Silke J, Walczak H, LUBAC prevents lethal dermatitis by inhibiting cell death induced by TNF, TRAIL and CD95L. Nat. Commun 9, 3910 (2018). [PubMed: 30254289]
55. Harris PA, Berger SB, Jeong JU, Nagilla R, Bandyopadhyay D, Campobasso N, Capriotti CA, Cox JA, Dare L, Dong X, Eidam PM, Finger JN, Hoffman SJ, Kang J, Kasparcova V, King BW, Lehr R, Lan Y, Leister LK, Lich JD, MacDonald TT, Miller NA, Ouellette MT, Pao CS, Rahman A, Reilly MA, Rendina AR, Rivera EJ, Schaeffer MC, Sehon CA, Singhaus RR, Sun HH, Swift BA, Totoritis RD, Vossenkamper A, Ward P, Wisnoski DD, Zhang D, Marquis RW, Gough PJ, Bertin J, Discovery of a first-in-class receptor interacting protein 1 (RIP1) kinase specific clinical candidate (GSK2982772) for the treatment of inflammatory diseases. J. Med. Chem 60, 1247–1261 (2017). [PubMed: 28151659]
56. Mifflin L, Hu Z, Dufort C, Hession CC, Walker AJ, Niu K, Zhu H, Liu N, Liu JS, Levin JZ, Stevens B, Yuan J, Zou C, A RIPK1-regulated inflammatory microglial state in amyotrophic lateral sclerosis. Proc. Natl. Acad. Sci. U.S.A 118, e2025102118 (2021). [PubMed: 33766915]
57. Weisel K, Scott N, Berger S, Wang S, Brown K, Powell M, Broer M, Watts C, Tompson DJ, Burriss SW, Hawkins S, Abbott-Banner K, Tak PP, A randomised, placebo-controlled study of RIPK1 inhibitor GSK2982772 in patients with active ulcerative colitis. BMJ Open Gastroenterol. 8, e000680 (2021).
58. Weisel K, Berger S, Thorn K, Taylor PC, Peterfy C, Siddall H, Tompson D, Wang S, Quattrocchi E, Burriss SW, Walter J, Tak PP, A randomized, placebo-controlled experimental medicine study of RIPK1 inhibitor GSK2982772 in patients with moderate to severe rheumatoid arthritis. Arthritis Res. Ther 23, 85 (2021). [PubMed: 33726834]
59. Weisel K, Berger S, Papp K, Maari C, Krueger JG, Scott N, Tompson D, Wang S, Simeoni M, Bertin J, Peter Tak P, Response to inhibition of receptor-interacting protein kinase 1 (RIPK1) in active plaque psoriasis: A randomized placebo-controlled study. Clin. Pharmacol. Ther 108, 808–816 (2020). [PubMed: 32301501]
60. Grievink HW, Heuberger J, Huang F, Chaudhary R, Birkhoff WAJ, Tonn GR, Mosesova S, Erickson R, Moerland M, Haddick PCG, Scearce-Levie K, Ho C, Groeneveld GJ, DNL104, a centrally penetrant RIPK1 inhibitor, inhibits RIP1 kinase phosphorylation in a randomized phase I ascending dose study in healthy volunteers. Clin. Pharmacol. Ther 107, 406–414 (2020). [PubMed: 31437302]
61. Liu Y, Chen YG, 2D- and 3D-based intestinal stem cell cultures for personalized medicine. Cell 7, 225 (2018).

62. Hsu N-Y, Nayar S, Gettler K, Talware S, Giri M, Alter I, Argmann C, Sabic K, Thin TH, Ko H-BM, Werner R, Tastad C, Stappenbeck T, Azabdaftari A, Uhlig HH, Chuang L-S, Cho JH, NOX1 is essential for TNFα-induced intestinal epithelial ROS secretion and inhibits M cell signatures. Gut 72, 654–662 (2022). [PubMed: 36191961]

63. Wu J, Cai Y, Wu X, Ying Y, Tai Y, He M, Transcardiac perfusion of the mouse for brain tissue dissection and fixation. Bio Protoc. 11, e3988 (2021).

64. Sauter M, Sauter RJ, Nording H, Olbrich M, Emschermann F, Langer HF, Protocol to isolate and analyze mouse bone marrow derived dendritic cells (BMDC). STAR Protoc. 3, 101664 (2022). [PubMed: 36097382]

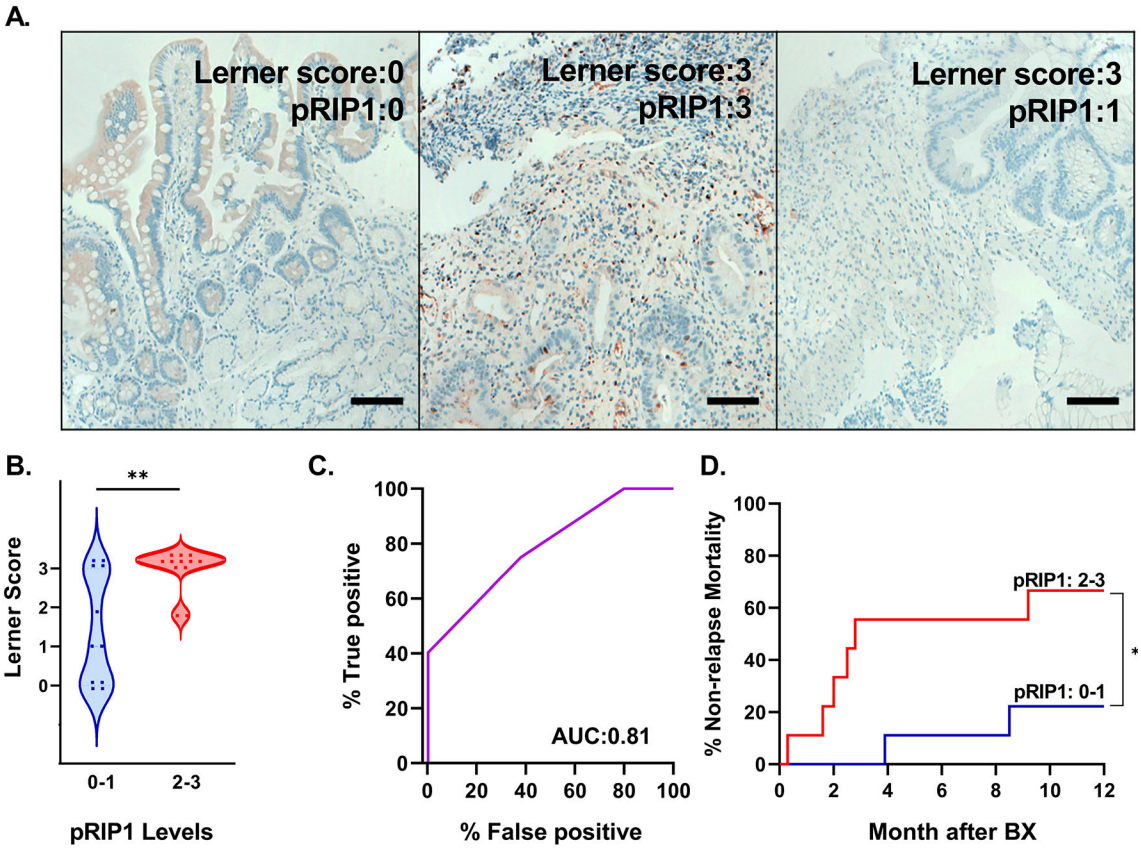

Fig. 1. RIP1 phosphorylation in gastrointestinal biopsies correlates with histologic damage and long-term outcomes.

(**A**) Immunohistochemistry of pRIP1 (Ser166) levels in 24 GI biopsies taken from patients with GI symptoms after HCT. Histologic severity was determined by the Lerner score. Scale bar, 100 μm. (**B**) Violin plot of pRIP1 abundance in GI biopsies that were classified as none/mild (0/1) or moderate/marked (2/3) and correlated the severity of damage as assessed by the Lerner score. (**C**) Receiving operator characteristic (ROC) curve of pRIP1 abundance and 12-month NRM after biopsy. (**D**) Cumulative incidence of NRM according to pRIP1 abundance. $^{**}P = 0.01$, unpaired two-tailed *t* test; $^{*}P = 0.027$, Log-rank (Mantel-Cox) test.

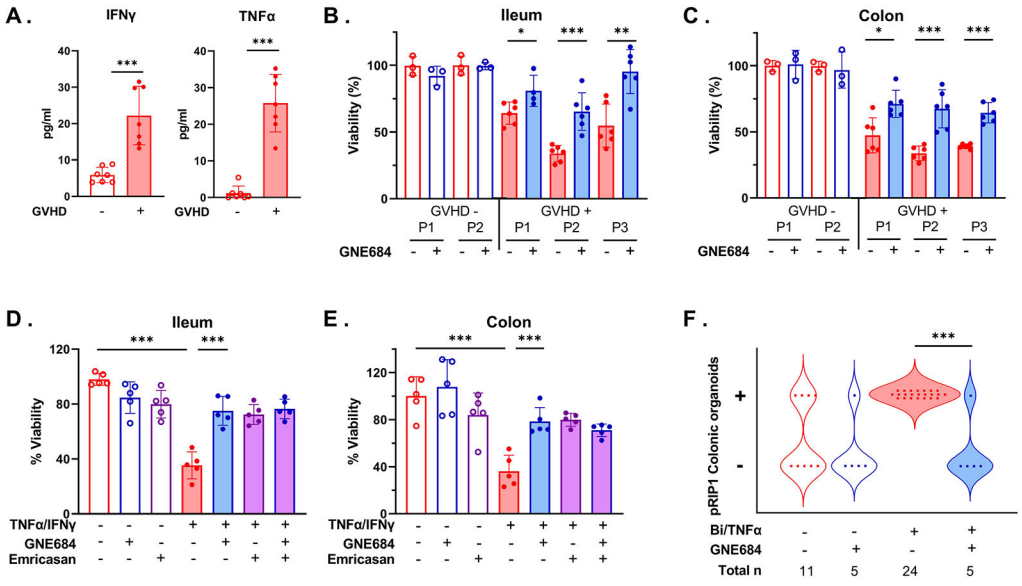

Fig. 2. Inactivation of RIP1 prevents apoptosis in human organoids.

(**A**) Concentrations of IFN-γ and TNFα in serum from patients with GVHD. (**B** to **E**) Organoids were established from healthy humans and cultured in media with the additives indicated as described in Materials and Methods. (B) Viability of ileal organoids 72 hours after the addition of serum from individual patients (P) either with no evidence of gastrointestinal GVHD (GVHD−) or with gastrointestinal GVHD symptoms (GVHD+). GNE684 was added to some cultures as described in Materials and Methods. (C) Viability of colonic organoids treated as in (B). (D and E) Viability of ileal and colonic organoids cultured with the indicated additives. (**F**) Organoids from human colons cultured in media with the additives as indicated and evaluated for pRIP1 by IHC as described in Materials and Methods. *$P < 0.05$, **$P < 0.01$, and ***$P < 0.001$, unpaired two-tailed t test.

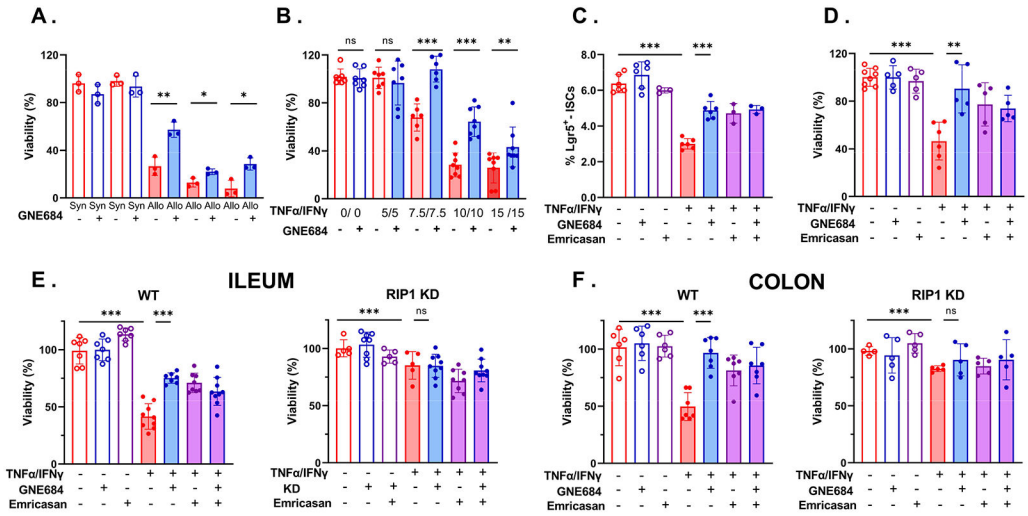

Fig. 3. Inactivation of RIP1 prevents apoptosis in murine organoids.

Organoids were established from mice as described in Materials and Methods and cultured in media with indicated treatments. (**A**) Sera from either syngeneic (open bars) or allogeneic (solid bars) transplanted mice were added to ileal mouse organoids, and viability was quantified as in Materials and Methods. (**B**) Viability in response to increasing concentrations of IFN-γ and TNFα. (**C**) Ileal organoids from Lgr5-eGFP mouse were established and treated as indicated; $Lgr5^+$ ISCs were quantified by flow cytometry. (**D**) Crypts from Lgr5-eGFP mice were dissociated into single cells and sorted to obtain $Lgr5^+$ ISCs; after sorting, ISCs were cultured with the additives indicated, and viability was assessed. (**E**) Ileal organoids from B6 WT mice (left) or B6-RIP1 KD mice (right) were cultured with the additives indicated, and viability was assessed as described in Materials and Methods. (**F**) Colonic organoids from B6 WT mice (left) or B6-RIP1 KD mice (right) were cultured as described in (E), and viability was assessed. $*P < 0.05$, $**P < 0.01$, and $***P < 0.001$, unpaired two-tailed *t* test.

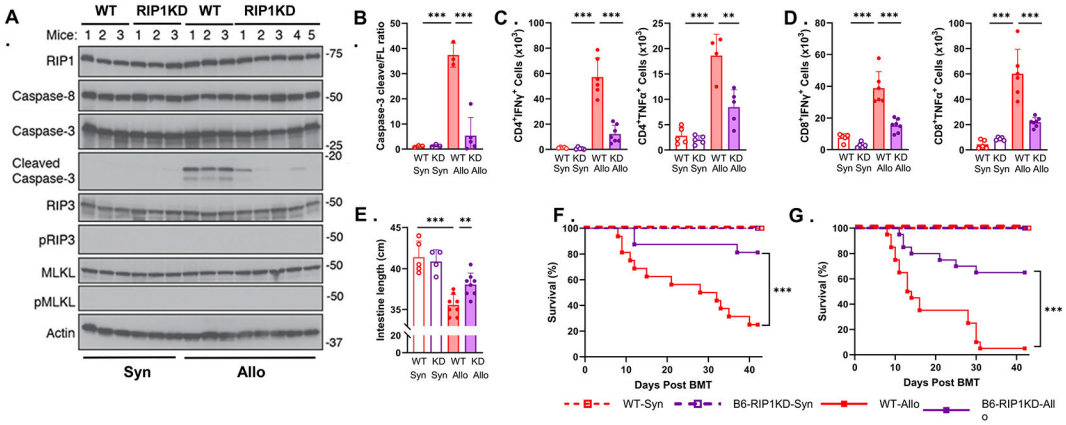

Fig. 4. Genetic inactivation of RIP1 in HCT recipient mice prevents GI GVHD and reduces mortality.

B6 WT and B6-RIP1 KD mice received HCT from syngeneic (open red and purple bars, respectively) or allogeneic C3H.SW donors (solid red and solid purple bars, respectively). Small intestines were harvested and analyzed on day 9 after HCT and Western blots, and flow cytometry of lamina propria lymphocytes was performed as described in Materials and Methods. (**A**) Western blots of ileum for RIP1, RIP3, pRIP3, MLKL, pMLKL, caspase 8, caspase 3, and actin from individual mice as indicated. (**B**) The ratio of cleaved caspase 3 to full-length (FL) caspase 3 as measured by densitometry. IFN-γ^+ and TNFα^+ were quantified for (**C**) CD4$^+$ and (**D**) CD8$^+$ populations. (**E**) Intestinal lengths were measured on day 9. (**F**) Survival of B6 WT recipients (solid red squares, $n = 16$) and B6-RIP1KD recipients (solid purple squares, $n = 16$) transplanted from C3H.SW donors and syngeneic B6 WT donors (open squares, $n = 7$ per group). (**G**) Survival of B6 WT HCT recipients (solid red squares, $n = 20$) and B6-RIP1KD HCT recipients (solid purple squares, $n = 20$) transplanted from allogeneic Balb/c donors and from syngeneic B6 WT donors (open red and purple squares, $n = 7$ per group). $^{**}P < 0.01$ and $^{***}P < 0.001$ [B to E: Unpaired two-tailed t test; F and G: Log-rank (Mantel-Cox) test].

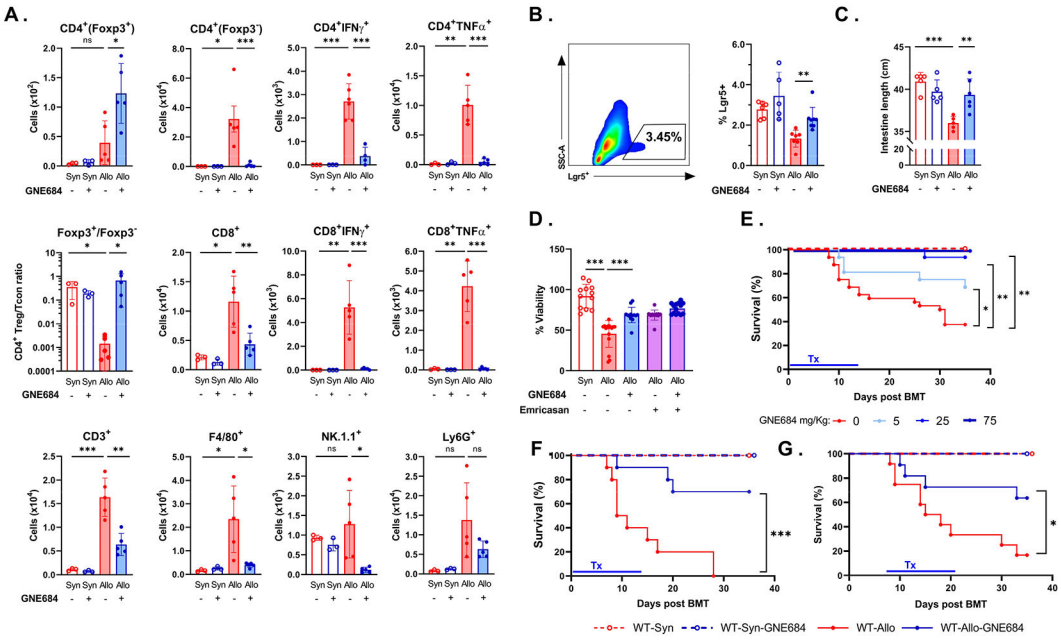

Fig. 5. Pharmacological inhibition of RIP1 by GNE684 prevents GI GVHD and improves survival in mice.

(**A** to **D**) B6 WT mice received HCT as in Fig. 4 and daily intraperitoneal injections of either GNE684 75 mg/kg (blue bars) or vehicle (red bars) from day 0 after HCT. (A) Intestines were processed on day 9 after HCT, and the numbers of leukocyte subpopulations in the lamina propria were analyzed and calculated by flow cytometry after syngeneic (open bars) or allogeneic (closed bars) HCT. Cellular subpopulations included the following: T lymphocytes ($CD3^+$), effector $CD4^+$ T cells ($CD4^+$IFN-γ^+ and $CD4^+TNF\alpha^+$), effector $CD8^+$ T cells ($CD8^+$IFN-γ^+ and $CD8^+TNF\alpha^+$), T_{regs} ($CD4^+Foxp3^+$), conventional T cells ($CD4^+Foxp3^-$), regulatory/conventional CD4+ T cell ratios ($Foxp3^+/Foxp3^-$), macrophages ($F4/80^+$), natural killer cells ($NK1.1^+$), and neutrophils ($Ly6G^+$). (B) ISCs of Lgr5-eGFP recipient mice as quantified by flow cytometry using the gating strategy described in Materials and Methods. (C) Small intestines were removed and measured from the proximal jejunum to the cecum. (D) Organoids from intestinal crypts of transplanted mice were cultured with additives as indicated, and viability was measured after 5 days. (**E**) Survival of B6 WT mice that received HCT from syngeneic B6 WT donors (open squares, $n = 6$ per group) or allogeneic C3H.SW donors (solid squares) that received 14 daily injections of GNE684 beginning on day 0 at the following doses (all in milligrams per kilogram): 0 (red, $n = 26$); 5 (light blue, $n = 16$); 25 (medium blue, $n = 16$); and 75 (navy blue, $n = 10$). (**F**) Survival of HCT recipients from syngeneic B6 WT donors (open circles, $n = 6$ per group) or from allogeneic Balb/c donors that received 14 daily injections from day 0 of either vehicle (red solid circles, $n = 10$) or GNE684 (75 mg/kg; blue solid circles, $n = 10$). (**G**) Survival of HCT recipients transplanted from syngeneic B6 WT donor (open circles, $n = 6$ per group) or from allogeneic C3H.SW donors (solid circles) that received 14 daily injections beginning on day +7 of either vehicle (red circles, $n = 10$) or GNE684 (75 mg/kg; blue circles, $n = 10$). Tx: daily injections, ns: nonsignificant, $*P < 0.05$, $**P < 0.01$, and $***P < 0.001$ [A to D: Unpaired two-tailed *t* test, E to G: Log-rank (Mantel-Cox) test].

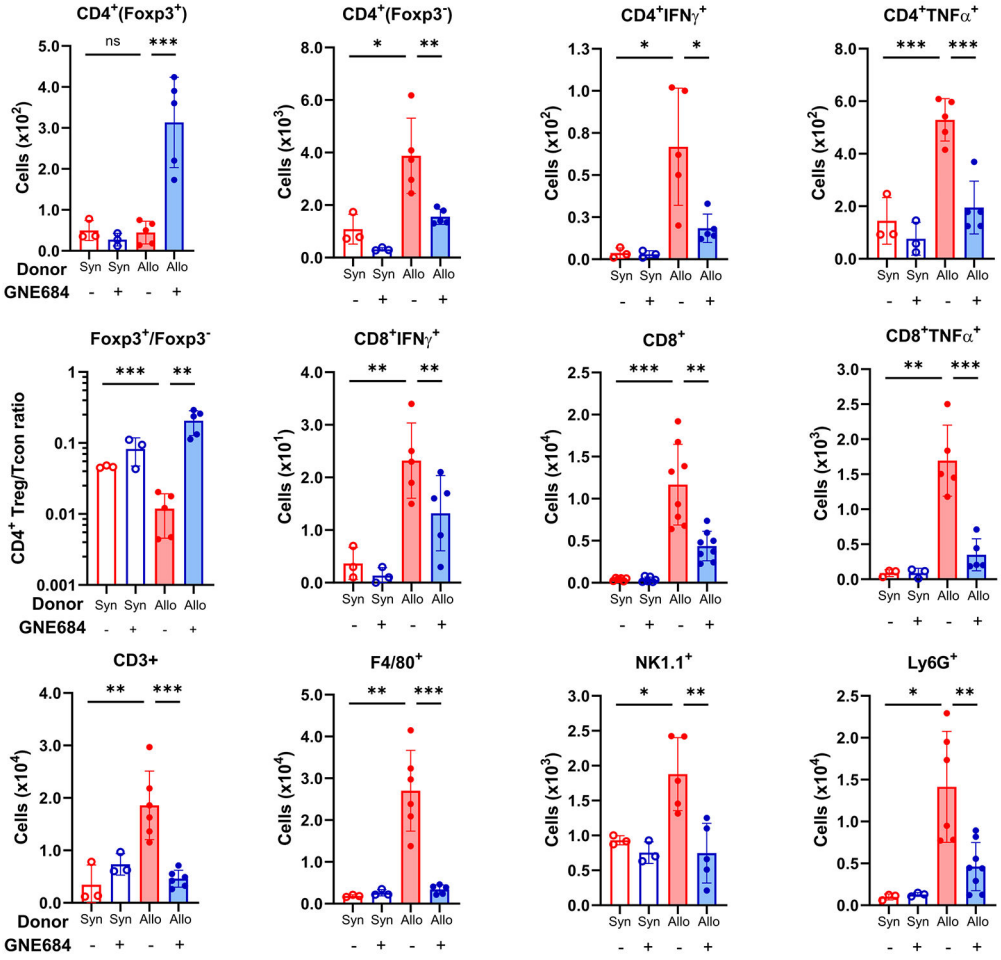

Fig. 6. Pharmacological inhibition of RIP1 by GNE684 prevents accumulation of inflammatory cellular infiltrates in mouse liver.

Mice were transplanted and treated as in Fig. 4. Livers were harvested on day 9 and processed, and the number of inflammatory cellular subpopulations was analyzed and calculated by flow cytometry as described in Materials and Methods. Cellular subpopulations included the following: T lymphocytes ($CD3^+$), effector $CD4^+$ T cells ($CD4^+IFN\text{-}\gamma^+$ and $CD4^+TNF\alpha^+$), effector $CD8^+$ T cells ($CD8^+IFN\text{-}\gamma^+$ and $CD8^+TNF\alpha^+$), T_{regs} ($CD4^+Foxp3^+$), conventional T cells ($CD4^+Foxp3^-$), regulatory/conventional CD4+ T cell ratios ($Foxp3^+/Foxp3^-$), macrophages ($F4/80^+$), natural killer cells ($NK1.1^+$), and neutrophils ($Ly6G^+$). ns, nonsignificant; $^*P < 0.05$; $^{**}P < 0.01$; $^{***}P < 0.001$, unpaired two-tailed *t* test.

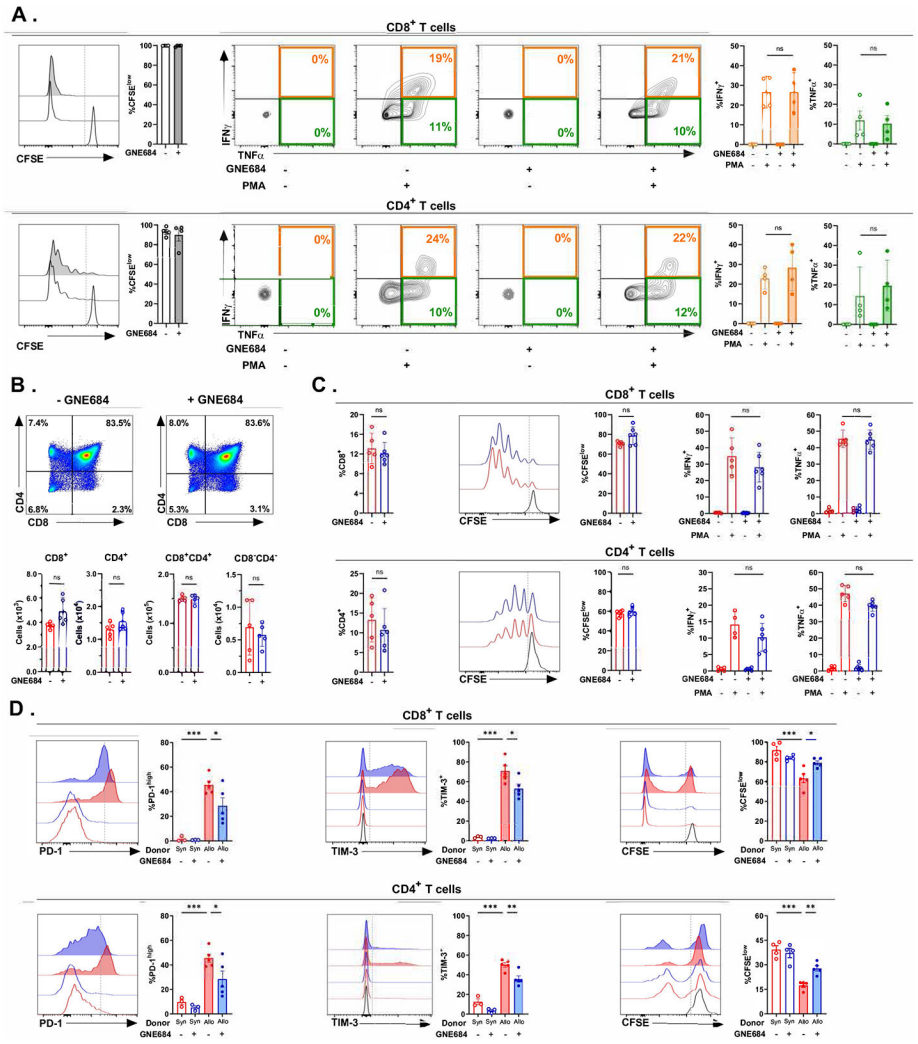

Fig. 7. Pharmacological inhibition of RIP1 by GNE684 does not suppress lymphocyte function and improves immune reconstitution during GVHD in mice.

(**A**) T cells isolated from naïve B6 WT mice were stained with CFSE and stimulated in vitro with antiCD3/CD28 beads with or without GNE684 for 5 days (left) and then stimulated with phorbol myristate acetate (PMA) for 4 hours to detect intracellular TNFα and IFN-γ (orange bars) or TNFα alone (green bars) (right). (**B** and **C**) B6 WT mice received HCT from syngeneic donors and were treated with vehicle or GNE684 75 mg/kg daily for 14 days (open red and blue bars, respectively), and organs were harvested on day 14. (B) Absolute numbers of $CD4^+$, $CD8^+$, $CD4^+CD8^+$, and $CD4^-CD8^-$ were quantified in the thymus by flow cytometry. (C) $CD3^+$ T cells were isolated and quantified from the spleen (left), stained with CFSE, and stimulated with antiCD3/CD28 beads in vitro for 5 days (middle). Cells were then harvested and stimulated with PMA for 4 hours to detect intracellular IFN-γ and TNFα by flow cytometry (right). (**D**) B6 WT mice received HCT from syngeneic (open bars) or allogeneic C3H.SW donors (solid bars) and were treated with vehicle or GNE684 75 mg/kg daily (red and blue bars, respectively). Splenocytes were isolated on day 14, and the cell surface expression of PD-1 and TIM-3 was analyzed for both $CD4^+$ and $CD8^+$ T cell subsets by flow cytometry (left and middle). $CD3^+$ T cells isolated from the splenocytes

were stained with CFSE, stimulated in vitro with Balb/c DCs for 5 days, and then analyzed for $CD4^+$ and $CD8^+$ cell surface expression (right). ns, nonsignificant; $*P < 0.05$; $**P < 0.01$; $***P < 0.001$ (A to D: Unpaired two-tailed *t* test).

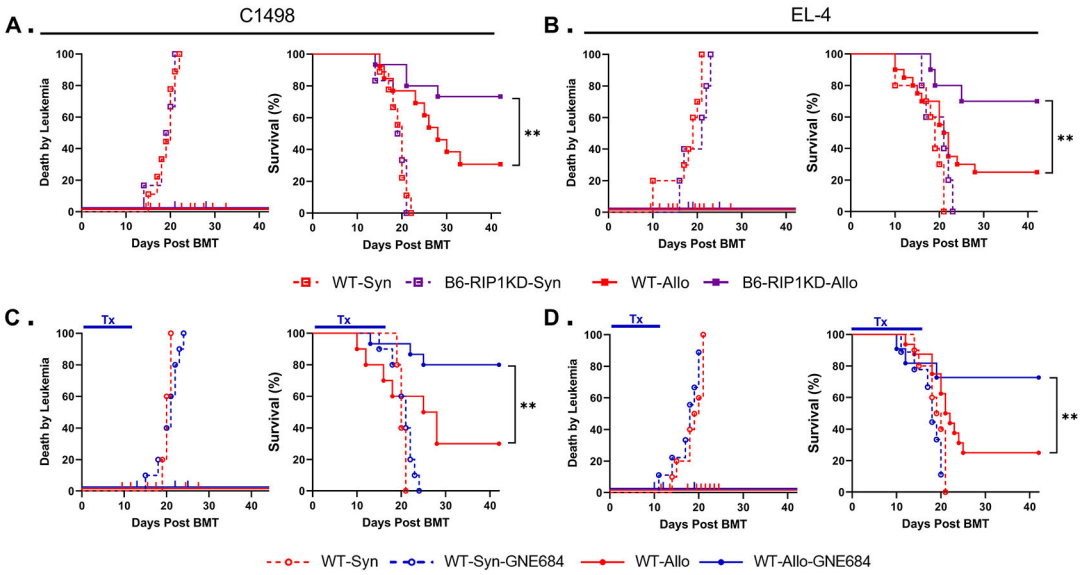

Fig. 8. RIP1 inhibition preserves GVL effects in mice.

Mice received HCT as in Fig. 4. A total of 5×10^5 C1498 (A and C) or 1×10^6 EL-4 (B and D) leukemia cells were added to the donor inoculum of each recipient. (**A** and **B**) Death by leukemia (left) and survival (right) of B6 WT recipients (red squares) and B6-RIP1 KD HCT recipients (purple squares) transplanted from syngeneic donors (open squares, $n = 15$ per group) or from allogeneic C3H.SW donors (solid squares, $n = 15$ per group). (**C** and **D**) Death by leukemia (left) and survival (right) of mice injected for 14 days intraperitoneally with vehicle (red solid circles, $n = 12$) or GNE684 (75 mg/kg; blue solid circles, $n = 17$) that received HCT from syngeneic B6 WT donors (open circles, $n = 15$ per group) and from allogeneic C3H.SW donors (solid circles). Mice that died from GVHD are shown as ticks along the x axis in the left panels. Tx: daily injections, $^{**}P < 0.02$ [Log-rank (Mantel-Cox) test].